



Wetland land cover change detection using multitemporal Landsat data: a case study of the Al-Asfar wetland, Kingdom of Saudi Arabia

Walid Chouari^{1,2}

Received: 24 August 2020 / Accepted: 22 February 2021 / Published online: 15 March 2021
© Saudi Society for Geosciences 2021

Abstract

The Al-Asfar wetland, locally known as Lake Al-Asfar, is the largest inland wetland in the Arabian Peninsula. It is situated to the east of the Al-Ahsa Oasis. It was formed at the expense of the Umm Hishah sabkha via the discharge of increasing quantities of drainage water to the oasis. This research was conducted to assess changes in land cover using four satellite images collected from 1990 to 2020. The study used a Landsat 5 TM image (1990), a Landsat 7 ETM+ image (2000), a Landsat 8 OLI-TIRS image (2010), and a Landsat Sentinel-2 L2A image to examine land cover in the Al-Asfar wetland. The normalized difference vegetation index (NDVI) and normalized difference water index (NDWI) were used to evaluate the tendency of ecosystem evolution. The results indicate that for the past three decades, the wetland area has increased significantly. Approximately 15.46 km² (24.69%) of the body of water was added during this time frame, and the vegetation areas expanded to approximately 10.74 km² (17.15%). The changes detected in the study area can be explained by the discharge of agricultural drainage water and semi-treated water from sewage treatment plants and the spread of reed mites (*Phragmites australis*) which covered approximately 23.81% of the area of the Al-Asfar wetland in 2020. For these reasons, the study recommends the necessity of imperative consideration for the protection of the resources of other wetlands in Saudi Arabia to ensure their sustainable use for future generations.

Keywords Al-Asfar · Landsat · NDVI · NDWI · Change detection

Introduction

Wetlands are important areas for the conservation of fauna and flora and production of economic income (Zhang et al. 2010; Rapinel et al. 2015; Youssef et al. 2009; Al-Dakheel et al. 2009; Fathi et al. 2009; Al-Sheikh and Fathi 2010; Ojaghi et al. 2017; Al-Obaid et al. 2017; Eid et al. 2020). Wetland conservation efforts were formulated under the Ramsar Convention after an abundance of studies related to the monitoring of wetlands were developed to help managers solve the many problems they face. The Al-Asfar wetland, which is part of the El Jafura dune field, has experienced significant evolutionary dynamic changes in recent decades

due to an increased inflow of agriculturally derived drainage water. At the Al-Ahsa Oasis, a 1450-km concrete irrigation system and a soil drainage system began operating in 1971. Drainage water is collected by the channel system and discharged into two wet depressions, namely, the Al-Asfar, and Al-Uyoun depressions (Fig. 1). The water collected in the drainage channel (D2) flows towards the sabkha of Al-Asfar 11 km east of the oasis. Between 1974 and 2018, the wetland received 2,186,407 m³ of water with a daily average input of 170,000 m³. The wetland has been negatively affected by the discharge of water polluted with chemical fertilizers (Al-Dakheel et al. 2009; Fathi et al. 2009; Al-Sheikh and Fathi 2010; Abdel-Moneim 2014). However, currently, the Al-Asfar depression provides a refuge for reed flora, acts as a habitat for wildlife, participates in flood protection, contributes to the reduction of the impact of water pollution, and aids the recharge of shallow groundwater (20 cm deep) (El Mahmoudi et al. 2011).

To study the evolution of this dynamic environment, image-processing techniques have been developed to extract water characteristics from satellite data. Various techniques of

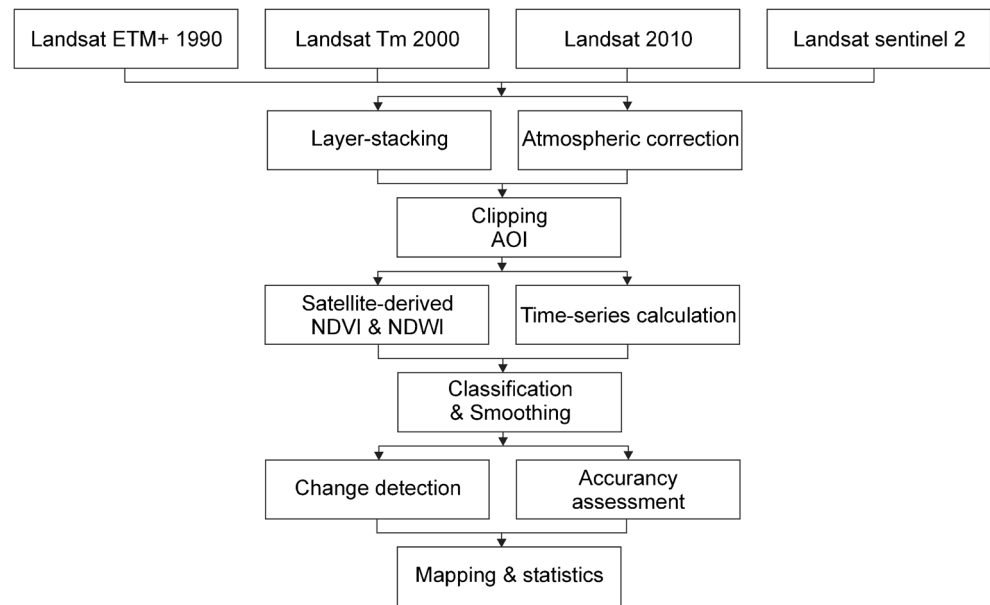
Responsible Editor: Stefan Grab

✉ Walid Chouari
wchouari@kfu.edu.sa; walidchouari@yahoo.fr

¹ Department of Social Studies, College of Arts, King Faisal University, P.O Box: 400, Al-Ahsa 31982, Saudi Arabia

² University of Sfax, Sfax, Tunisia

Fig. 1 Flowchart of the methodological procedures followed in this study



surface water extraction were first examined in this study (McFeeters 1996). This research aims to assess the spatio-temporal dynamics of the Al-Asfar wetland over the period of 1990–2020 using Landsat TM, ETM+, OLI, and Sentinel multitemporal data. The article evaluates the use of NDWI and NDVI to assess the importance of the evolution of the Al-Asfar wetlands to inform decision-makers about these developments and improve future management of depressions.

Materials and methods

To accomplish the objectives of this research, the outlined steps were followed: the study area was delimited, a database was created using under Arc GIS, satellite images were preprocessed using ERDAS Imagine, indices capable of detecting water bodies were tested, the wetland was delimited in each scene, and the land use/land cover dynamics were evaluated. Figure 1 explains the procedures followed in this research to distinguish wetland changes.

Study area

The Al-Asfar depression is one of the most famous wetlands in the Arabian Peninsula. It is located east of the Al-Ahsa oasis. The depression used to be a sabkha, referred to as the Umm Hishah sabkha, which was fed spring water, storm water, and groundwater near the surface. The wetland is now fed by the discharge of partially treated agricultural drainage water from the oasis and participates in the protection of the oasis against the dynamics of sand dunes (Fig. 2).

The basin of Al-Ahsa is characterized by a general slope that inclines towards the northeast. The irrigation and drainage canals

follow this direction and flow into the Al-Asfar wetland. In the west, the elevation at the outlet of channel D2 does not exceed 113 m above mean sea level. The average altitude is 103 m in the central part of the depression and 94 m in the eastern part. The Al-Asfar wetland is highly reliant on the amount of water drained, which is conveyed through channel D2. It is subject to annual and seasonal fluctuations. Generally, during the summer, evaporation contributes to reductions in the water level of the depression and consequential increase in salinity.

On the banks of the wetland, current dynamics, characterized by a constant conflict between water and sand, have produced jagged and continuously changing shores. The water body is subdivided into three main zones: a western zone covering 7.7 km², a central zone dismantled, covering 3.1 km² which is subject to strong wind activity, and finally a western zone covering 4.41 km². The three zones are connected by wide passages. The large supply of drainage contributes to the flooding of flat shores and spread of salinity.

Processing and analysis methodology of satellite images

A technique for extracting wetland characteristics was used to model spatial-temporal changes in the Al-Asfar wetland over the period of 1990–2020 using multitemporal Landsat images (Tuxen et al. 2011; Kaptué et al. 2013; Rokni et al. 2014; Chen et al. 2014; Huang et al. 2014; Petropoulos et al. 2015; Nhu et al. 2020; Eid et al. 2020). Therefore, identification of the different land cover classes was performed for the years of 1990 and 2020 using a maximum likelihood classification algorithm. The two designated indices, NDVI and NDWI, were examined and studied independently (using thresholds specific to each image) to extract the wetland area during each

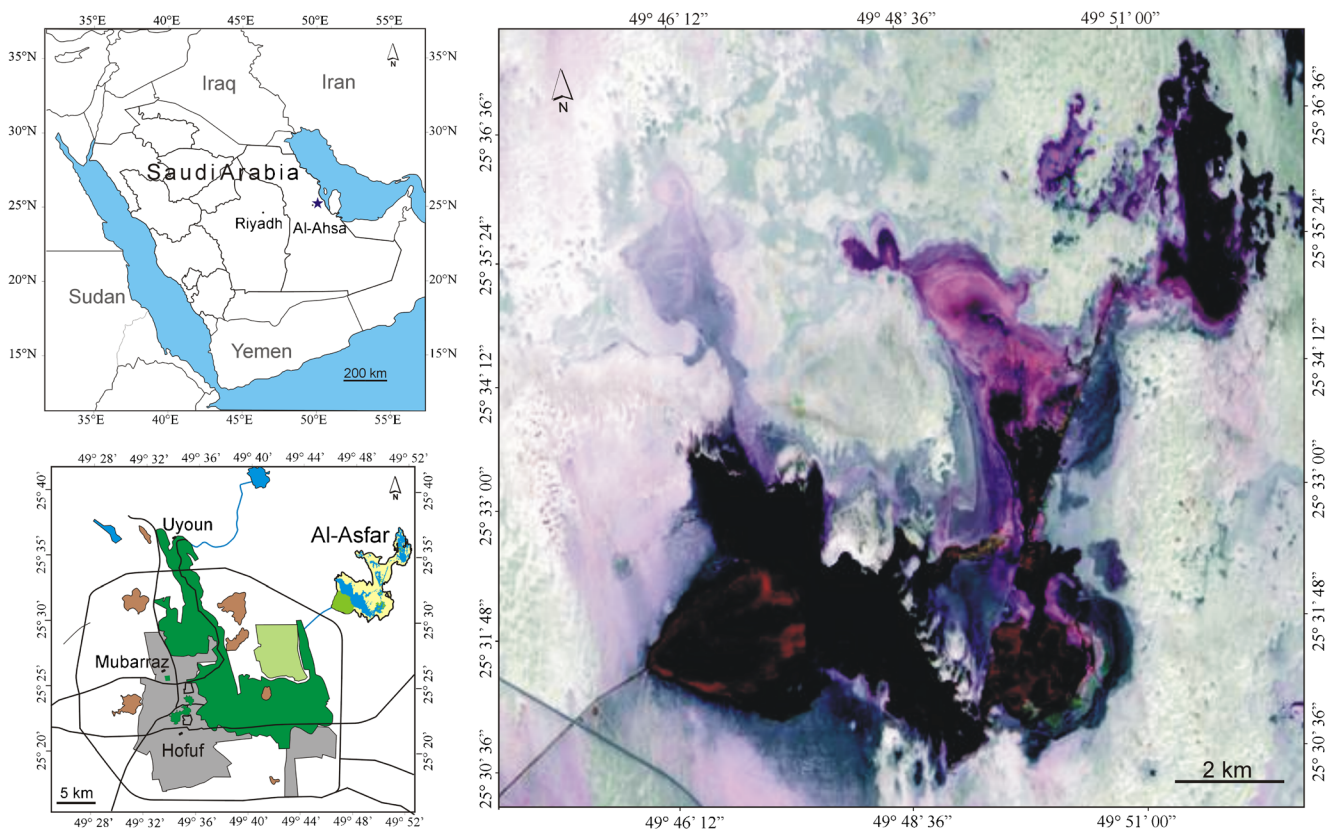


Fig. 2 Study area

date (Zoffoli et al. 2008; Dong et al. 2014). Finally, the maps generated were superimposed to produce a map of wetland area’s evolution during the 1990–2020 period.

Pre-processing

The research exploited four types of satellite imagery, Landsat TM (Thematic Mapper), ETM+ (Enhanced Thematic Mapper Plus), OLI-TIRS (Operational Land Imager-Thermal Infrared Sensor), and Sentinel satellite images. These images were downloaded from the US Geological Survey site. These images were used to examine spatio-temporal changes in land use/land cover in the Al-Asfar wetland. All satellite images were obtained during the summer season (during the clear days of June and July) to mitigate the effects of clouds and

seasonal variations on the processing of satellite images and guarantee the quality of the results obtained (Table 1).

The research was undertaken for three decades to understand the state of the ecosystem of Al-Asfar. Twenty ground control points (GCPs) were taken throughout field investigations using a Global Positioning System (GPS) to evaluate the diverse stages of data treatment for change detection and field verification (Fig. 1). These ground control points (GCPs) were used in the geometric correction of the selected satellite images. The process of correcting satellite data is an essential step in the superposition and analysis of multi-source and multiscale data. When capturing satellite images, they are distorted by the projection, tilt angle of the sensor, atmospheric condition, curvature of the Earth’s surface, and local topography. To overlay classified maps, analyse the results of change detection, and derive expressive statistics,

Table 1 Characteristics of Landsat TM, ETM+, OLI+TIRS, and Sentinel-2 data

Satellite	Sensor	Path/row	Acquisition date	Spatial resolution
Landsat 5	TM	164/042	15-07-1990	30 m
Landsat 7	ETM+	164/042	02-07-2000	15 m
Landsat 8	OLI + TIRS	164/042	28-06-2010	15 m
Landsat	Sentinel-2 L2A	164/042	28-06-2020	10 m

geometric distortions must be corrected or rectified in the same map projection (Fontinovo et al. 2012; Gianinetto 2012; Wang et al. 2012; Nguyen 2015).

Accordingly, raw remote sensing images cannot be used directly with mapping products in a geographic information system. The most widely applied model is based on the use of ground control points (GCPs) to achieve high geodetic accuracies. Geometric corrections explicitly implement mapping functions using ground control points (GCPs) and determine the brightness of pixels in a corrected image (Wang et al. 2012). The GCPs are an important data source for geometry correction by remote sensing. Thus, the satellite images were georeferenced using a topographic sheet at a scale of 1:25000 and rectified according to the WGS 1984 datum (World Geodetic System) and the Universal Transverse Mercator (UTM) coordinate system to guarantee consistency between satellite data during the analysis phase.

Geometrically corrected Landsat images were imported into ERDAS Imagine after overlapping individual strip layers. The combined bands provided a colour composition for all Landsat datasets. This included bands 7, 4, and 2 for the Landsat TM images, which signify red, green, and blue (RGB); bands 3, 2, and 1 for the Landsat ETM+ image; bands 7, 5, and 3 for the Landsat OLI+TIRS image; and bands 4, 3, and 2 for the Sentinel 2 image. In addition, a subset of images was created to define the “area of interest” (AOI) that was digitalized on the screen from the selected images. The images were cut by a space analyst tool (extracted by a mask). In addition, a subset of images was created in Arc GIS to delineate the area of interest (AOI) based on a vector shape file of the perimeter of the wet depression.

Processing

A classification system was applied to estimate the impact of land cover/land use changes over a 30-year period from 1990 to 2020. The first image used TM captures from 1990 with a spatial resolution of 30 m (Table 1). This resolution was improved with the use of the Sentinel-2 satellite image. The spectral bands used for the two satellite images were green, red, and near-infrared. On the basis of these three bands, a false colour composite image was produced. These bands are commonly used for land cover mapping and vegetation discrimination. After selecting the channels that were subjected to classification, training areas were selected by digitizing polygons of homogeneous surface areas. Based on the knowledge of the field, the ground control points (GCPs) were located on each image. The identification of the different land cover classes was carried out using a maximum likelihood classification algorithm.

Other studies have used both NDVI, NDWI, and NDMI to detect changes in wetlands such as Zoffoli et al. (2008), Dong et al. (2014), Gandhi et al. (2015), Mousazadeh et al. (2015),

Das (2017), Ojaghi et al. (2017), Kadhim (2018), Ahangarha et al. (2019), and Eid et al. (2020). All of the aforementioned studies noted that there were expressive changes in the NDVI, NDWI, and NDMI values throughout the study period. The calculation of NDVI relies on the fact that chlorophyll in vegetation strongly absorbs radiation in the visible range of red light and robustly reflects radiation in the near-infrared range of the spectrum. Hence, NDVI is defined as the normalized relationship between reflection in the near-infrared (NIR) range and red portions of the spectrum (Zoffoli et al. 2008; Peters et al. 2002; Dong et al. 2014; Ke et al. 2015; Shao et al. 2016). Other scholars have applied NDVI to evaluate vegetation cover (Shao et al. 2016), observe vegetation trends, and monitor agrarian drought (Peters et al. 2002). NDVI is a measurement index applied to the management of natural resources that offers indications concerning the monitoring of crop cover evolution and plant growth stages (Bhandari et al. 2012; Rokni et al. 2014). In addition, NDVI can be used to effectively extract water bodies from Landsat data. In this index, near-infrared (NIR) represents the nearby infrared reflectance in a section of the band. Red is the reflectance in the red portion of the band. NDVI values range between -1 and $+1$ and are distributed between positive values which indicate green vegetation, and negative or near zero values, representing nonvegetated land covers, such as deserts, water bodies, and urban areas. Open soil areas have a similar reflectance in the aforementioned two bands, and the resulting NDVI is near zero (Chen et al. 2014).

NDWI was proposed by McFeeters (1996). NDWI is used to detect changes relevant to the water content of water surfaces. This satellite-derived index is calculated as the ratio difference between the calculated canopy reflectance of the green band response and the near-infrared band response for each pixel in a satellite image. In general, near-infrared (NIR) bands are able to detect the moisture content of soil and vegetation and, then, are valuable in wetland detection (McFeeters 1996; Xu 2006; Eid et al. 2020). The index is sensitive to built-up land and can overestimate water bodies. NDWI increases with increasing water contents in leaves or when moving from dry soil to open water. The use of NDWI humidity masks, generated from Landsat images, has multiple benefits. These masks make it possible to avoid nonhumid zones and thus allow a more precise detection of effective wet zones (Sheng et al. 2016; Table 2).

To extract the best features, NDVI and NDWI values range from $+1$ to -1 . However, NDMI is a normalized difference moisture index that exploits NIR and SWIR bands to extract moisture. NDMI is used to control variations in water content in water bodies based on the NIR and SWIR wavelengths (McFeeters 1996). In addition, NDMI was established for the exploration of vegetation-water liquids and thus would not be efficient extracting water features. Indeed, this is related to the type of image tested, the season during which the image

Table 2 The most common satellite-derived indices applied for water feature extraction (in Landsat imagery: green, band 2; red, band 3; NIR (near-infrared), band 4; MIR (middle-infrared), band 5; and SWIR (shortwave-infrared), band 7) (Rokni et al. 2014)

Indices	Equations	Remarks
Normalized difference vegetation index	$NDVI = (NIR - Red)/(NIR + Red)$	Water has a negative value
Normalized difference water index	$NDWI = (Green - NIR)/(Green + NIR)$	Water has a positive value
Normalized difference moisture index	$NDMI = (NIR - SWIR)/(NIR + SWIR)$	Water has a positive value

is taken, and the land cover/land use classes in the image. Accordingly, the best practice for obtaining the best values for the indices applied in this study (NDVI and NDWI) is to experiment with diverse edge values. Table 3 presents the NDVI intervals and concordant classes in accordance with the classification advanced by the Foundation of Remote Sensing Phenology.

The NDWI and NDVI values were defined using the selected Landsat images and classified according to the unsupervised iso-cluster classification. The results were exploited to confront variations in wetland extension during the selected dates. The different extracted NDVI values were also reclassified into three essential classes: vegetation, no vegetation, and open soil. In addition, the different NDWI values were reclassified into three classes: water bodies, hydromorphic areas, and non-aqueous areas. The NDWI class for hydromorphic areas corresponded to the NDVI class for open soil areas (Table 4). The Arc Map calculation tool was used to define the zoning of the six detected classes of NDVI and NDWI.

In this regard, NDWI and NDVI were defined from the TM 1990, ETM + 2000, OLI + TIRS 2010, and Sentinel-2 L2A 2020 images to assess their performance in water body extraction. An edge was applied to group the pixels into land and water bodies. Appropriate land-water edges for the two indices were defined by comparison with reference maps produced by visual photointerpretation.

The rationale behind using this classification method was to detect the two main components of the Al-Asfar wetland: water bodies and vegetated areas. The vegetation class covered all plant species in the Al-Asfar depression, of which 95% consisted of reed beds such as *Phragmites australis*, *Halocnemum strobilaceum*, *Zygophyllum mandavillei*, and *Haloxylon salicornicum* (Youssef et al. 2009). The open soil class was described as “bare sand dune areas.” The water body corresponds to the water surface of the Al-Asfar wetland. This classification made it possible to compare changes in the wetland over the last three decades.

Table 3 NDVI value range in accordance with data from the Foundation for Remote Sensing Phenology (US Geological Survey)

NDVI value	Class
≤ 0.1	Very low NDVI
0.2 to 0.5	Moderate NDVI
0.6 to 0.9	High NDVI

Change detection

To determine land cover changes in the Al-Asfar wetland during the period of 1990–2020, the water body of the study area was defined individually in all selected images. Consequently, the relevance of indices derived from the satellite, such as NDWI and NDVI, was inspected for the determination of water bodies from Landsat data (Rokni et al. 2014).

The phase of numerical determination of changes corresponds to the process of estimating differences in the land use/land cover classes across the four dates. This process supplies the ability to measure temporal effects using multispectral image data. Pixel-to-pixel and post-classification comparisons are two application methods that reflect the advantages of remote sensing. They ensure automatic detection of changes by confronting images of the same area taken on different dates (Othman et al. 2013; Tuxen et al. 2011; Rokni et al. 2014; Chen et al. 2014; Huang et al. 2014; Petropoulos et al. 2015; Prasad and Ramesh 2019; Eid et al. 2020).

The method of post-classification detection is among the most suitable and commonly applied techniques for detecting changes (Tuxen et al. 2011; Rokni et al. 2014; Chen et al. 2014; Huang et al. 2014; Petropoulos et al. 2015). This method was used to confront three scenes of change in 1990, 2000, and 2010 based on that observed in 2020. It easily offers a change matrix in which transfers from one land use/land cover type to another can be visually estimated. This method begins with the classification step that generates classified images that recognize change surfaces as pixel-by-pixel differences in class membership (Acharya et al. 2017; Buma et al. 2018).

Table 4 NDVI and NDWI classes for the Al-Asfar wetland

NDVI values	Classes	NDWI values	Classes
−1 to 0.1	No-vegetation	0.2 to 1	Water body
0.1 to 0.2	Open soil	0 to 0.2	Hydromorphic surfaces
0.2 to 1	Vegetation	−1 to 0	Non-aqueous surfaces

Results and discussion

Land use/land cover status in the Al-Asfar wetland

Land use/land cover was mapped for 1990, 2000, 2010, and 2020 to study the changes that have occurred over the past 30 years. Figure 3 shows a superimposed map resulting from vector maps of the Al-Asfar wetland dated 1990, 2000, 2010, and 2020, as well as AOI maps for the Landsat multitemporal satellite images of the wetland.

The implementation of new satellite sensors in the optical domain characterized by high spatial resolution such as Sentinel-2 makes it possible to envisage, in particular, a detailed mapping of land cover. Water surfaces are distinguished from other landscape elements by a strong absorption in the wavelengths of the near and middle infrared. This is manifested in the image by dark areas. The visual interpretation of the coloured compositions, of the Sentinel-2 image made with false colour channels (Red8, SWIR1, Red), shows the richness of its informative content, especially for the detection of wetlands. The processed satellite images (1990 and 2020) made it possible to differentiate nine land cover classes: water bodies, sabkhas, hydromorphic surfaces, vegetated areas, barchan dunes, barchanoid ridges, transverse dunes, dune

complexes, and nabka dunes. Three of the land cover classes, i.e., water bodies, vegetated areas, and sand dunes, each have a distinctive spectral behaviour in the two satellite images used. However, the differentiation between the six remaining classes is sometimes not perfect and can therefore induce confusion. Likewise, the comparison between the two contingency matrices produced for 1990 and 2020 displays an enhancement in the distinction of the land cover classes. The mean of this distinction was assessed at 78 and 85 for the land cover maps of 1990 and 2020, respectively. Thus, there is an improvement in the accuracy of the land cover map of the most recent date (2020) compared to that mapped on the older date (1990). In addition, with a reduced number of classes (<3), the results are generally better. The classification confusion noted comes from the choice of samples based on the objects resulting from poor pixel aggregation. The confusion between water and vegetation is explained by the fact that the water is very rich in nutritious algae and the vegetation is very discontinuous, which makes them difficult to individualize.

The comparison of the different land cover classes between 1990 and 2020 highlights a significant dynamic in the Al-Asfar wetland. There was a positive trend between these two dates in the water body (200%) and vegetated areas (300%). This dynamic is mainly explained by the conflict between

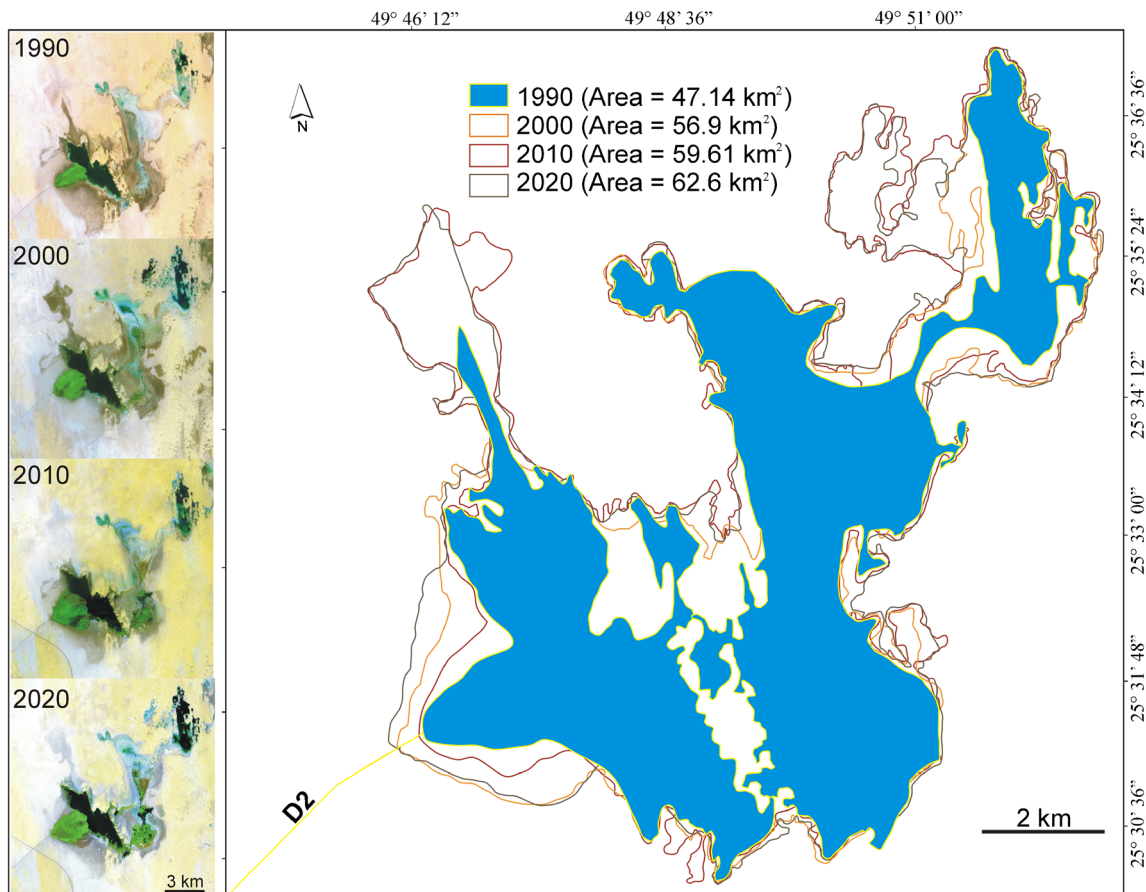


Fig. 3 Variation in the shoreline and area of the Al-Asfar wetland in 1990, 2000, 2010, and 2020

water and sand. The progression of the water body was detrimental to the sand dunes and their response to the increase in the quantities of water drained towards the depression.

The accuracy of the land use/land cover classification was widely acceptable for all classes mapped. However, inaccuracies are noted in the sand dune form classes, and that correspond to nabka dunes or hydromorphic surfaces. Then, this classification implies detailed knowledge of the information that will be extracted, and various tests are necessary for defining the optimal segmentation parameters (Fig. 4).

Furthermore, precision assessment analyses show that NDMI was unable to extract the water body from the Al-Asfar wetland, although NDWI and NDVI produced the most accurate maps. It appears that the errors in the maps are generally focused around the banks of the wetland and overlaps between water bodies and hydromorphic surfaces. As a result, NDVI and NDWI were used to model spatial-temporal changes in the Al-Asfar wetland over the period of 1990–2020. The wetland area was extracted by classification according to NDWI and NDVI using thresholds specific to each image. Finally, multirate maps of wetland area were superimposed to produce maps of changes in the wetland area over the period of 1990–2020. Figures 5 and 6 show the classified NDVI and NDWI maps of the Al-Asfar wetland for the selected dates in 1990, 2000, 2010, and 2020, respectively.

Analysis of the classification results shows that NDVI subdivided the study area into three surfaces: the first surface without vegetation indicates the wetland water body; the second surface is open soil; and the third surface is vegetation. NDWI also classifies the study area into three surfaces: the water body surface, the hydromorphic surface (water soaked) that corresponds to the open soil class of NDVI, and the non-aqueous surface class that corresponds to the vegetation class of NDVI.

Tables 5 and 6 present the areas in square kilometre and percentage of each class covering the wet depressions for the four selected dates. In Table 4, the no-vegetation class corresponds to the water surface class in Table 5. Additionally, the change detection of the open soil class was not analysed given the change in the boundary of the study area between 1990 and 2020. The comparison of the NDVI and NDWI classes shows that the error between the no-vegetation zone in NDVI and the water body zone in NDWI is 9.19%, which is acceptable.

The detailed situation of land use/land cover in the Al-Asfar wetland is as follows over three decades; the water body and vegetation classes reflected positive growth; however, the open soil class (hydromorphic surfaces) showed a positive and negative trend in the Al-Asfar wetland due to the change in the boundary of the depression.

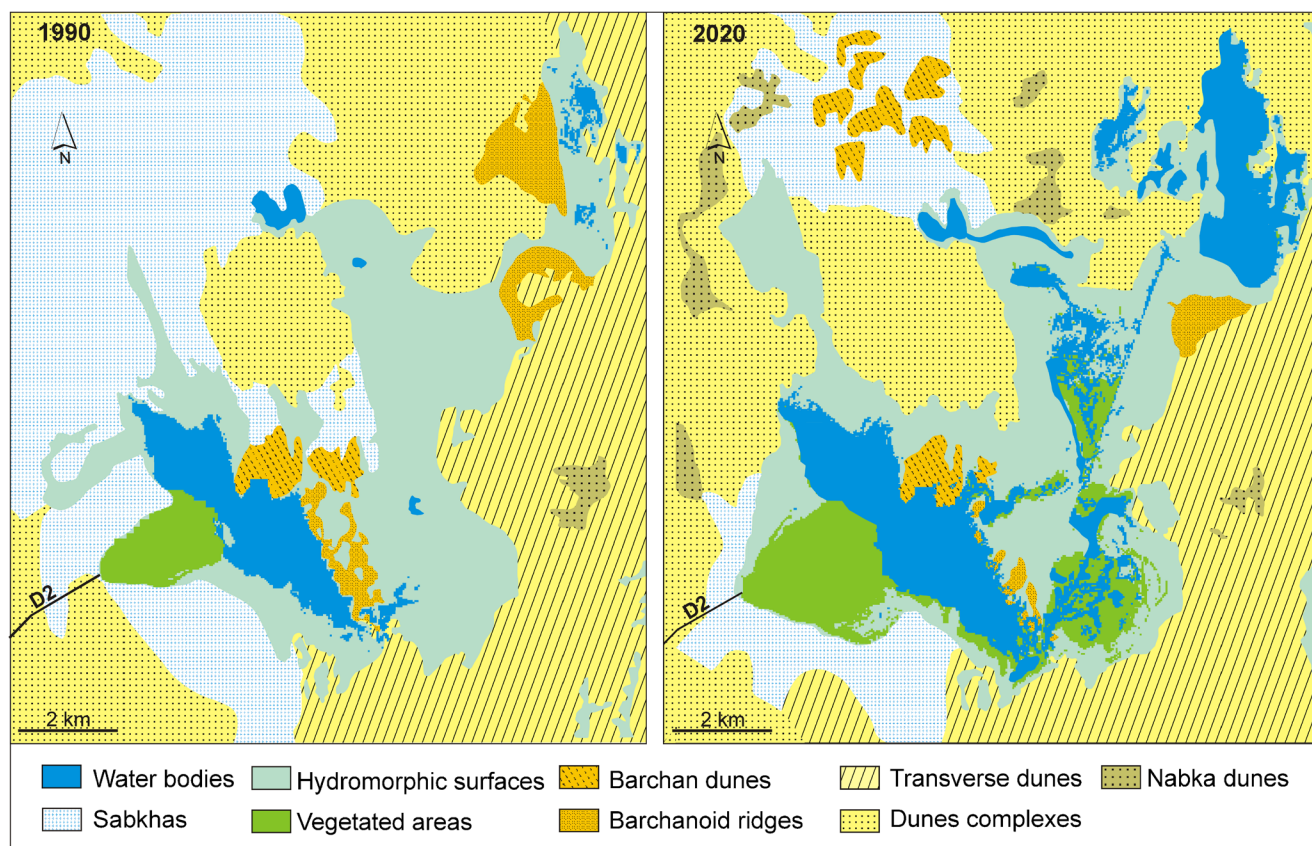
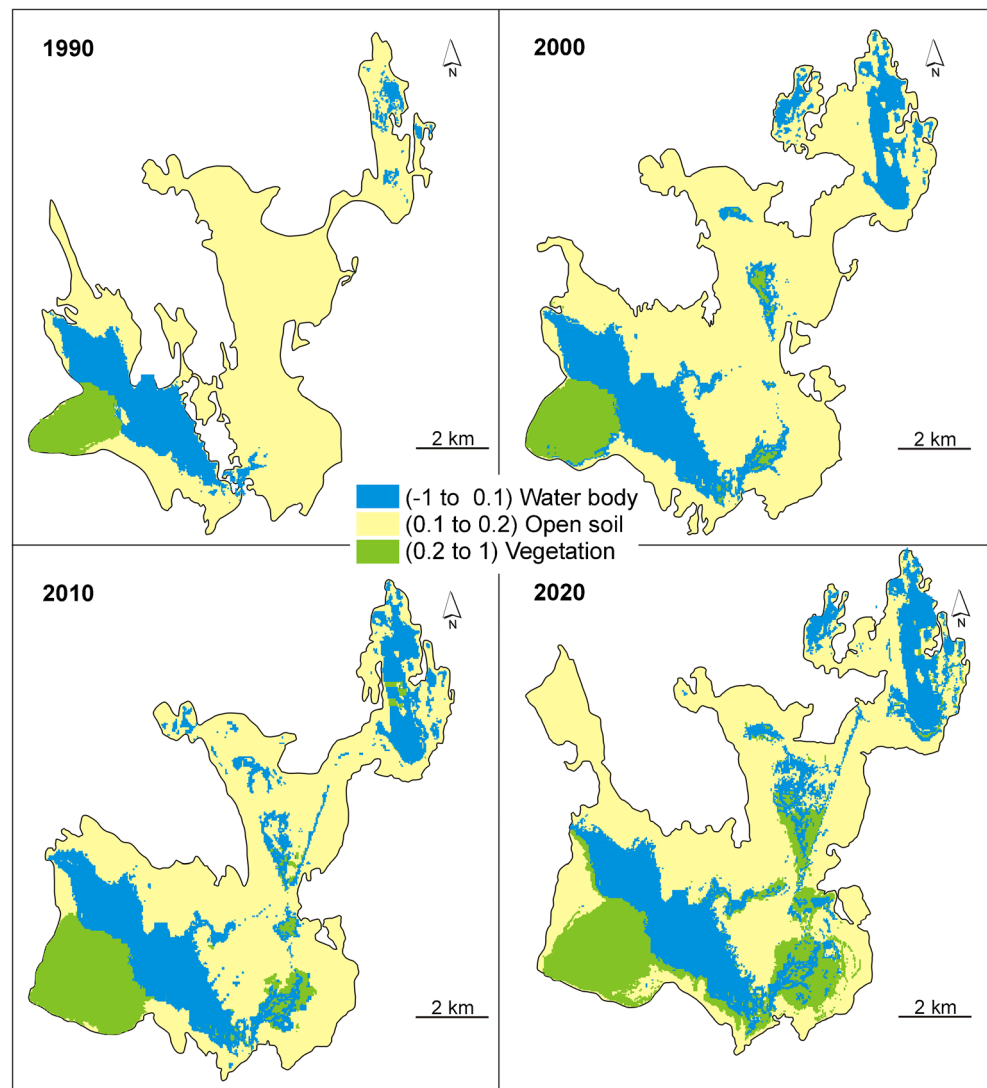


Fig. 4 Land use/land cover of the Al-Asfar wetland in 1990 and 2020

Fig. 5 NDVI maps for the Al-Asfar wetland dated 1990, 2000, 2010, and 2020



Water body This is the most dynamic type of land cover, accounting for 7.74 km² (16.42%) of the overall Al-Asfar wetland area in 1990. The surface water area amounted to 15.21 km² (24.3%) in 2020. The wetland doubled its water body over the past 30 years at an annual average rate of +0.25 km² between 1990 and 2020, although the annual rate of increase decreased between 2010 and 2020 (+0.73 km²). This extension of the water body was attributed to the increased inflow of drainage water into the wetland and opening of new drains through the sand dunes.

Vegetation This land use/land cover class showed considerable expansion in comparison with the water body class over the past three decades. The overall extent of the vegetation class increased from 4.17 km² (8.85%) in 1990 to 14.91 km² (23.82%) in 2020. This represents an increase in the area occupied by reed beds (mainly, *Phragmites australis*, *Typha*, and *Juncus actus*). The continued development of this

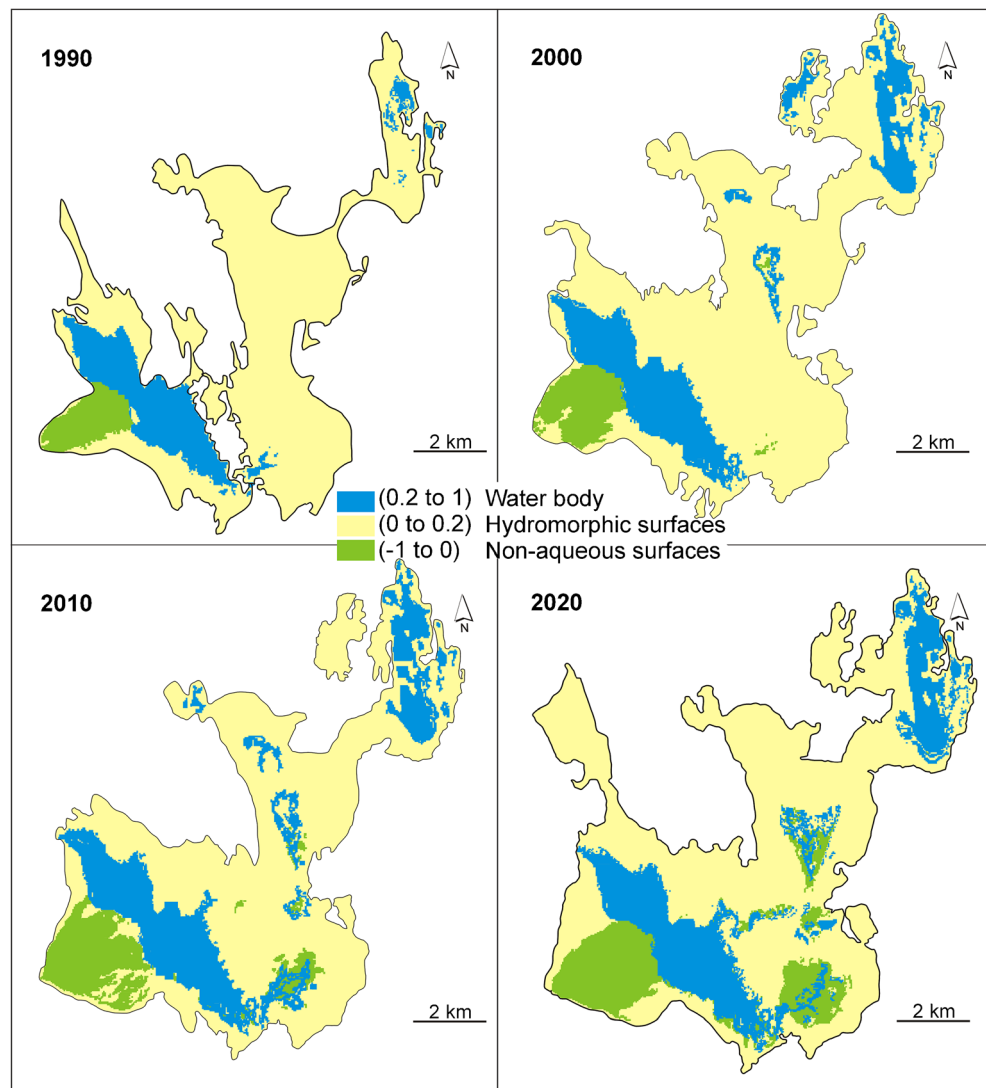
vegetation has led to the drying of parts of the wetland, including the shallowest areas, and conversion of the wetland into connected islands.

Change detection analysis

On the basis of the 2020 data, land cover evolution detection was performed to reveal the transformations occurring for the 1990–2020, 2000–2020, and 2010–2020 periods using of the NDVI and NDWI, as presented in Figs. 7 and 8. Statistics from the classification method applied showed that there was a marked increase in the total area of the wetland, as shown in Tables 5 and 6. The area of the depression was 47.14 km² in 1990, and it increased to 62.6 km² in 2020 because of the rise in the quantity of water discharged (Fig. 3).

Change detection maps were produced to show changes among the three compared intervals of 1990–2020, 2000–2020, and 2010–2020 (Figs. 7 and 8).

Fig. 6 NDWI maps for the Al-Asfar wetland dated 1990, 2000, 2010, and 2020



Analysis of the change results of the changes shows that between 1990 and 2020, the total increase in the wetland, vegetation class, and water surface class areas was 15.46 km², 10.74 km², and 7.47 km², respectively, and the total decrease in the open soil class (sand dunes) area was 2.75 km² (Table 6).

The area of the water body class was 7.74 km² in 1990; however, it amounted to 15.46 km² in 2020. Of the area of the water body class, approximately 11.78

km² remained unchanged, 4.35 km² changed within the vegetation zone, and 8.03 km² changed within the open soil class. Most of the water body class changed to the open soil class due to the wind dynamics and consequent dune accumulations.

The inflow of effluents, fertilizers, and agricultural nutrients into the Al-Asfar wetland caused the eutrophication of the water body and the growth of reed beds. The total area of vegetation was 4.17 km² in 1990; it expanded to 14.91 km²

Table 5 NDVI classes in km² and percentages in the Al-Asfar wetland

Class name	1990		2000		2010		2020	
	Area (km ²)	%	Area (km ²)	%	Area (km ²)	%	Area (km ²)	%
Water body	7.74	16.42	11.29	23.36	14.48	24.29	15.21	24.30
Vegetation	4.17	8.85	6.72	8.30	9.92	16.64	14.91	23.82
Total	11.91	25.27	18.01	31.66	24.4	40.93	30.12	48.12

Table 6 Detection of NDVI class changes for the Al-Asfar wetland in 1990, 2000, and 2010 based on 2020

Class name	1990–2020		2000–2020		2010–2020	
	Area (km ²)	%	Area (km ²)	%	Area (km ²)	%
Water body → no change	6.2	13.15	9.17	16.12	11.78	19.76
Water body → vegetation	1.33	2.82	1.92	3.37	0.34	0.57
Water body → open soil	0.21	0.45	0.2	0.35	2.36	3.96
Vegetation → no change	4.15	8.80	5.64	9.91	5.57	9.34
Vegetation → water body	0.02	0.04	0.7	1.23	0.75	1.26
Vegetation → open soil	0	0.00	0.38	0.67	3.6	6.04
Open soil → water body	3.55	7.53	9.06	15.92	4.11	6.89
Open soil → vegetation	10.51	22.30	8.23	14.46	3.92	6.58
Total	25.97	55.09	35.3	62.03	29.43	54.4

in 2020. Of the entire area of vegetation, approximately 5.57 km² remained unchanged (in 2020), 0.75 km² shifted to the water surface class, and 3.6 km² shifted to the open soil class (Table 7).

Fig. 7 Detection of changes in NDVI in the Al-Asfar wetland in 1990, 2000, and 2010 based on 2020

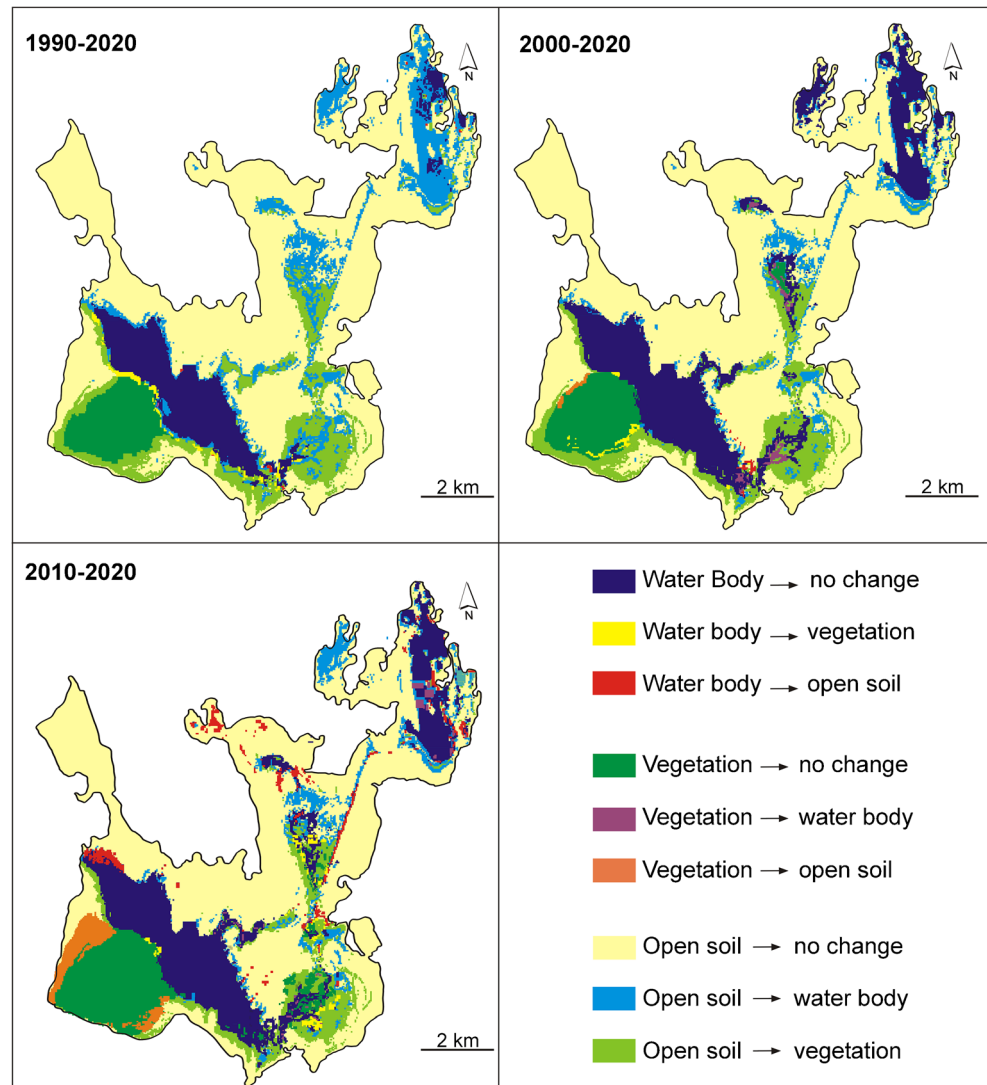
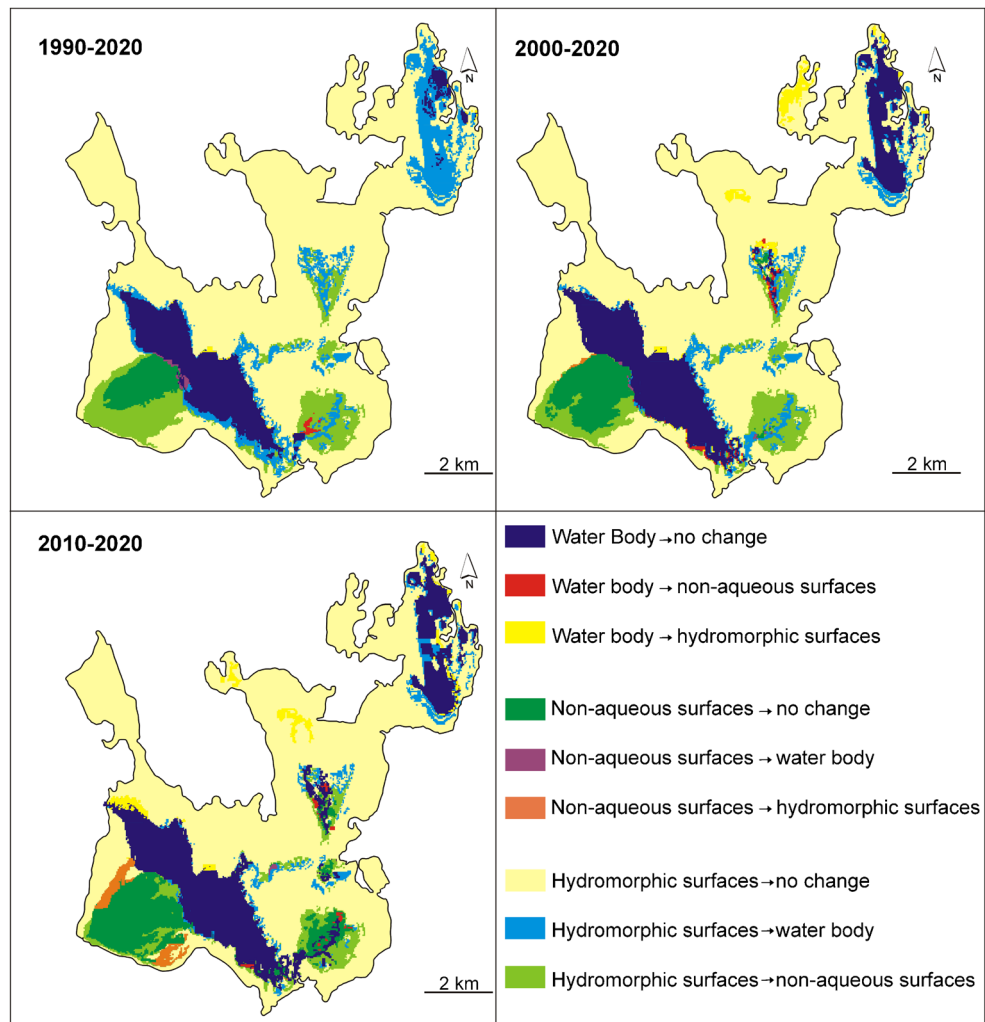


Fig. 8 Detection of changes in NDWI for the Al-Asfar wetland in 1990, 2000, and 2010 based on 2020



Accuracy assessment

NDVI was essentially proposed for separating green crop cover areas from other land covers. Nevertheless, it did achieve good water body detection results. Water features improved

by using NDWI are frequently mixed with the open soil class, and thus the area of extracted water can be overestimated (Rokni et al. 2014). Table 8 presents an assessment of the kappa statistics and overall accuracy of the NDVI method covering the selected dates in 1990, 2000, 2010, and 2020.

Table 7 Detection of NDWI class changes for the Al-Asfar wetland in 1990, 2000, and 2010 based on 2020

Class name	1990–2020		2000–2020		2010–2020	
	Area (km ²)	%	Area (km ²)	%	Area (km ²)	%
Water body → no change	5.11	10.84	8.11	14.25	11.22	18.85
Water body → non-aqueous surfaces	0.27	0.57	0.45	0.79	0.28	0.47
Water body → hydromorphic surfaces	0.13	0.28	0.64	1.12	2.45	4.12
Non-aqueous surfaces → no change	2.83	6.00	3.45	6.06	7.51	12.62
Non-aqueous surfaces → water body	0.25	0.53	0.15	0.26	0.1	0.17
Non-aqueous surfaces → hydromorphic surfaces	0	0.00	0.22	0.39	2.3	3.86
Hydromorphic surfaces → water body	6.41	13.60	5.11	8.98	4.03	6.77
Hydromorphic surfaces → non-aqueous surfaces	9.76	20.70	8.02	14.09	3.98	6.69
Total	24.76	52.52	26.15	45.94	31.97	53.55

Table 8 Overall accuracy and kappa statistics of NDVI and NDWI for 1990, 2000, 2010, and 2020

Dates	NDVI		NDWI	
	Overall accuracy	Kappa statistics	Overall accuracy	Kappa statistics
1990	91	0.89	88	0.85
2000	91	0.89	90	0.88
2010	92	0.93	91	0.89
2020	98	0.95	97	0.95

The overall accuracy and the kappa statistics are 91% and 0.89 in 1990, 91% and 0.89 in 2000, 92% and 0.93 in 2010, and 98% and 0.95 in 2020, respectively. However, that of the NDWI classified images are 88% and 0.85, 90% and 0.88, 91% and 0.89, and 97% and 0.95, respectively. These statistics reflect that the different ranked maps meet the minimum recommended overall accuracy of 85%. They also show that there is remarkable symmetry between the reference data and the land use/land cover classification according to the selected indices (Foody 2002) (Table 8).

This study may be of interest because it shows the dynamics of the two main land cover types in the Al-Asfar depression: water surface and vegetation. The overall results enhance the understanding of the causes and factors of the evolution of the Al-Asfar wetland. The results of this mapping study revealed that the water surface class of the Al-Asfar depression is continuously increasing. The area is exposed to the dangers of flooding at the expense of adjacent farmland, salinity spread, and rising water table levels.

Due to the extent and pervasiveness of the land cover change effects in the Al-Asfar wetland, scholars are invited to objectively assess past public policies and decision-making processes. Management policies should consider practical actions that can allow the Al-Asfar wetland to adapt to anthropogenic interventions and natural dynamics to improve its adaptive capacity and reduce anthropogenic disturbances and actions that influence the components of the wetland. Such research helps to comprehend the recent status of the study area by confronting historical and recent Landsat images. This research can also help to make predictions about the future that can subsequently direct environmental decisions, particularly in the area of optimizing water use in this arid environment.

Conclusion

Remote sensing methods offer a precise, fast, and cost-effective technique to detect changes in wetlands. These methods solve the problems encountered when applying traditional techniques that are hard to implement and time-

consuming (aerial photographs and topographical maps). Land use/land cover classification maps realized by an unsupervised iso-cluster classification method revealed changes in the different resulting classes in the study area. The water body and vegetation class developed the most in favour of the open soil class. The optimized use of land use/land cover information is indispensable for the implementation of land use/land cover plans to establish links between water bodies, sand dunes, soil, flora, and fauna. The results revealed that the Al-Asfar ecosystem underwent significant transformations in land use/land cover between 1990 and 2020. The influence of land cover change affects approximately 50% of the total area of the Al-Asfar wetland over these three decades. Additionally, there have been observable increases in the water surface and vegetation classes. Approximately 18.21 km² of open soils were lost due to the conversion to vegetated areas and water bodies; however, the area of vegetation increased by 10.74 km². Therefore, this research proposes crucial considerations to decision-makers regarding the protection of residual wetland resources, to take the needed actions to reduce ecological risks for this wetland, thus improving the sustainable usage of the water body due to its worldwide importance and conserving its threatened biodiverse species.

Acknowledgements The author acknowledges the Deanship of Scientific Research at the King Faisal University for the financial support under Nasher Track (Grant No. 206033).

Compliance with ethical standards

Conflict of interest The author declares that he has no competing interests.

References

- Abdel-Moneim A (2014) Histopathological and ultrastructural perturbations in tilapia liver as potential indicators of pollution in Lake Al-Asfar, Saudi Arabia. *Environ Sci Pollut Res* 21:4387–4396
- Acharya TD, Yang IT, Anoj Subedi A, Lee DH (2017) Change detection of lakes in Pokhara, Nepal Using Landsat Data. *Proceedings* 1:17. <https://doi.org/10.3390/ecsa-3-E005>

- Ahangarha M, Seydi ST, Reza Shahhoseini R (2019) Hyperspectral change detection in wetland and water-body areas based on machine learning, the International Archives of the Photogrammetry, Remote Sensing and Spatial Information Sciences, GeoSpatial Conference 2019 – Joint Conferences of SMPR and GI Research, Volume XLII-4/W18: 19-24
- Al-Dakheel YY, Hussein AHA, El-Mahmoudi AS, Massoud MA (2009) Soil, water chemistry and sedimentological studies of Al Asfar evaporation lake and its Inland sabkha, Al-Hassa area, Saudi Arabia. *Asian J Earth Sci* 2:1–21
- Al-Obaid S, Samraoui B, Thomas J, El-Serehy HA, Alfarhan AH, Schneider W, O'Connell M (2017) An overview of wetlands of Saudi Arabia: Values, threats, and perspectives. *Ambio* 46:98–108. <https://doi.org/10.1007/s13280-016-0807-4>
- Al-Sheikh H, Fathi AA (2010) Ecological studies on Al-Asfar Lake. Al-Hassa, Saudi Arabia, with special references to the sediment. *Res J Environ Sci* 4:13–22
- Bhandari A, Kumar A, Singh GK (2012) Feature extracting using normalized difference vegetation index (NDVI): a case study of Jabalpur city. *Proc Technol* 6:612–621
- Buma WG, Lee S, Seo JY (2018) Recent surface water extent of lake Chad from multispectral sensors and GRACE. *Sensors* 18:2082. <https://doi.org/10.3390/s18072082>
- Chen L, Jin Z, Michishita R, Cai J, Yue T, Chen B, Xu B (2014) Dynamic monitoring of wetland cover changes using time-series remote sensing imagery. *Ecol Inform* 24:17–26
- Das K (2017) NDVI and NDWI based change detection analysis of Borfoibam Beelmukh Wetlandscape, Assam using IRS LISS III data. *ADB-U J Eng Technol* 6(2)
- Dong Z, Wang Z, Liu D, Song K, Li L, Jia M, Ding Z (2014) Mapping wetland areas using Landsat-derived NDVI and LSWI: a case study of West Songnen plain, Northeast China. *J Indian Soc Remote Sens* 42:1–8
- Eid A, Olatubara CO, Ewemoje TA, Farouk H, El-Hennawy MT (2020) Coastal wetland vegetation features and digital change detection mapping based on remotely sensed imagery: El-Burullus Lake, Egypt. *Int Soil Water Conserv Res* 8:66–79
- El Mahmoudi AS, Massoud MA, Al-Dakheel YY, Hussein AHA (2011) Studies of Al Asfar and Al Yououn evaporation lakes water quality and the potential of its reuse in agriculture activities, Al Hassa Area, KSA; JKAU: Met., Env. and Arid Land Agric Sci 22, 3: 67-85 (2011 A.D. /1432 A.H.). 10.4197/ Met. 22-3.4
- Fathi AA, Al-Fredan MA, Youssef AM (2009) Water quality and phytoplankton communities in Lake Al-Asfar, AL-Hassa, Saudi Arabia. *Res J Environ Sci* 3:504–513
- Fontinovo G, Allegrini A, Atturo C, Salvatori R (2012) Speedy methodology for geometric correction of MIVIS data. *Eur J Remote Sens* 45:19–25. <https://doi.org/10.5721/EuJRS20124502>
- Foody GM (2002) Status of land cover classification accuracy assessment. *Remote Sens Environ* 80(1):185–201. [https://doi.org/10.1016/S0034-4257\(01\)00295-4](https://doi.org/10.1016/S0034-4257(01)00295-4)
- Gandhi GM, Parthiban S, Thummalu N, Christy A (2015) NDVI: Vegetation change detection using remote sensing and GIS-a case study of Vellore District. *Proc Comput Sci* 57:1199–1210
- Gianinetto M (2012) Automatic co-registration of satellite time series, the. *Photogramm Rec* 27(140):462–470. <https://doi.org/10.1111/j.1477-9730.2012.00689.x>
- Huang C, Peng Y, Lang M, Yeo IY, Mccarty G (2014) Wetland inundation mapping and change monitoring using Landsat and airborne LiDAR data. *Remote Sens Environ* 141:231–242
- Kadhim MM (2018) Monitoring land cover change using remote sensing and GIS techniques: a case study of Al-Dalmaj Marsh, Iraq. *J Eng* 9(24):96–108
- Kaptué AT, Hanan NP, Prihodko L (2013) Characterization of the spatial and temporal variability of surface water in the Soudan-Sahel region of Africa. *J Geophys Res* 118:1–12
- Ke Y, Im J, Lee J, Gong H, Ryu Y (2015) Characteristics of Landsat 8 OLI-derived NDVI by comparison with multiple satellite sensors and in-situ observations. *Remote Sens Environ* 164:298–313
- McFeeters SK (1996) The use of the normalized difference water index (NDWI) in the delineation of open water features. *Int J Remote Sens* 17:1425–1432
- Mousazadeh R, Ghaffarzadeh H, Nouri J, Gharagozlou A, Farahpour M (2015) Land use change detection and impact assessment in Anzali international coastal wetland using multi-temporal satellite images. *Environ Monit Assess* 187:776. <https://doi.org/10.1007/s10661-015-4900-0>
- Nguyen TH (2015) Optimal ground control points for geometric correction using genetic algorithm with global accuracy. *Eur J Remote Sens* 48(1):101–120. <https://doi.org/10.5721/EuJRS20154807>
- Nhu VH, Mohammadi A, Shahabi H, Shirzadi A, Al-Ansari N, Bin Ahmad B, Chen W, Khodadadi M, Ahmadi M, Khosravi K, Jaafari A, Nguyen H (2020) Monitoring and assessment of water level fluctuations of the Lake Urmia and its environmental consequences using multitemporal Landsat 7 ETM+ Images. *Int J Environ Res Public Health* 17:4210. <https://doi.org/10.3390/ijerph17124210>
- Ojaghi S, Ahmadi FF, Ebadi H, Bianchetti R (2017) Wetland cover change detection using multi-temporal remotely sensed data; a case study: Ghara Gheshlagh wetland in the southern part of the Urmia Lake. *Arab J Geosci* 10:470. <https://doi.org/10.1007/s12517-017-3239-y>
- Othman AA, Al-Saady YI, Al-Khafagi AK, Gloaguen R (2013) Environmental change detection in the central part of Iraq using remote sensing data and GIS. *Arab J Geosci* 7(3):1017–1028
- Peters AJ, Walter-shea EA, Ji L, Vina A, Hayes M, Svoboda MD (2002) Drought monitoring with NDVI-based standardized vegetation index. *Photogramm Eng Remote Sens* 68(1):71–75
- Petropoulos GP, Kalivas DP, Griffiths HM, Dimou PP (2015) Remote sensing and GIS analysis for mapping spatio-temporal changes of erosion and deposition of two Mediterranean river deltas: the case of the Axios and Aliakmonas rivers, Greece. *Int J Appl Earth Obs* 35: 217–228
- Prasad G, Ramesh MV (2019) Spatio-temporal analysis of land use/land cover changes in an ecologically fragile area—Alappuzha District, Southern Kerala, India; *Natural Resources Research*, 28, S1. <https://doi.org/10.1007/s11053-018-9419-y>
- Rapinel S, Bouzillé JB, Oszwald J, Bonis A (2015) Use of bi-seasonal Landsat-8 imagery for mapping marshland plant community combinations at the regional scale. *Wetlands* 35:1–12
- Rokni K, Ahmad A, Selamat A, Hazini S (2014) Water feature extraction and change detection using multitemporal Landsat imagery. *Remote Sens* 6:4173–4189. <https://doi.org/10.3390/rs6054173>
- Shao Y, Lunetta RS, Wheeler B, Liames JS, Campbell JB (2016) An evaluation of time-series smoothing algorithms for land-cover classifications using MODIS-NDVI multi-temporal data. *Remote Sens Environ* 174:258–265
- Sheng Y, Song CH, Wang J, Lyons EA, Knox BR, Cox JS, Gao F (2016) Representative lake water extent mapping at continental scales using multi-temporal Landsat-8 imagery. *Remote Sens Environ* 185: 129–141. <https://doi.org/10.1016/j.rse.2015.12.041>
- Tuxen K, Schile L, Stralberg D, Siegel S, Parker T, Vasey M, Callaway J, Kelly M (2011) Mapping changes in tidal wetland vegetation composition and pattern across a salinity gradient using high spatial resolution imagery. *Wetl Ecol Manag* 19:141–157
- Wang J, Yong Gea Y, Heuvelink G, Zhoua C, Brusd D (2012) Effect of the sampling design of ground control points on the geometric

- correction of remotely sensed imagery. *Int J Appl Earth Obs Geoinf* 18:91–100
- Xu H (2006) Modification of normalised difference water index (NDWI) to enhance open water features in remotely sensed imagery. *Int J Remote Sens* 27(14):3025–3033. <https://doi.org/10.1080/01431160600589179>
- Youssef AM, Al-Fredan MA, Adel A, Fathi AA (2009) Floristic composition of Lake Al-Asfar, Alahsa, Saudi Arabia. *Int J Bot* 5:116–125. <https://doi.org/10.3923/ijb.2009.116.125>
- Zhang L, Wang MH, Hu J, Ho YS (2010) A review of published wetland research, 1991–2008: Ecological engineering and ecosystem restoration. *Ecol Eng* 36:973–980
- Zoffoli ML, Kandus P, Madanes N, Calvo DH (2008) Seasonal and interannual analysis of wetlands in South America using NOAA-AVHRR NDVI time series: the case of the Parana Delta region. *Landsc Ecol* 23:833–848